Magnesium Technology 2013
Edited by: Norbert Hort, Suveen N. Mathaudhu, Neale R. Neelameggham, and Martyn Alderman
TMS (The Minerals, Metals & Materials Society), 2013

TAILORING PRECIPITATES IN Mg-6Zn-2Gd BASED ALLOY SUBJECTED TO HIGH PRESSURE TORSION

J.H. Li[1*], P. Schumacher[1, 2]

[1*] Chair of Casting Research, Department of Metallurgy, University of Leoben, A-8700, Leoben, Austria (jie-hua.li@hotmail.com)
[2] Austrian Foundry Research Institute, Parkstrasse 21, Leoben, Styria, A-8700, Austria

Keywords: Mg-Zn-Gd alloy; Age hardening; Precipitate; TEM; High pressure torsion.

Abstract

The precipitates formed at lower ageing temperatures are very unstable at higher application temperatures, thus are not ideal for the high temperature applications. A traditional approach in solving the problem is from alloy design and development route by increasing solute concentrations or addition of micro-alloying elements. Recently, high pressure torsion was also employed to tailor the precipitate microstructures of the age-hardening alloy that are significantly different from those obtained by conventional isothermal ageing treatments. In this contribution, an Mg-6Zn-2Gd-0.4Zr (wt. %) alloy has been subjected to high pressure torsion (HPT). The precipitate microstructure evolution during HPT processing has been characterised using TEM, with an aim to elucidate the effect of HPT processing on nucleation and growth of precipitates, and the mechanisms dominating the evolution of precipitate microstructure. This investigation demonstrates a new perspective for application of HPT to tailor precipitate microstructure for unique properties in service.

Introduction

Magnesium alloys have great potential for the application in automotive and aerospace application due to their high specific strength [1]. The Mg-Zn based alloys, i.e. ZK51 (Mg-4.5Zn-0.6Zr (wt. %)), have been widely used as a wrought Mg alloy. However, the precipitates formed in binary Mg-Zn alloys during artificial ageing are generally coarse and inhomogeneously distributed [2]. The high temperature mechanical properties of Mg-Zn binary alloys, especially the creep-resistant properties, become inadequate for technological applications at a temperature above 250 °C. Research on the age hardening behaviour of Mg-Zn based alloy is of great importance to further improve the age hardening response by controlling the decomposition of the supersaturated solid solution of Zn in Mg [3].

Mg-Zn-Gd system was thought to be promising to develop high strength Mg alloys since precipitates can be formed on the basal plane [4, 5, 6] or both on the prismatic and basal plane [7]. Especially, an Mg-6Zn-2Gd (wt. %, short for ZG62) alloy has been reported to have increased mechanical properties [8, 9]. Above 200°C, the TYS and UTS of ZG62 alloy is slightly higher than that of a Gd-free alloy. More importantly, the elongation of the ZG62 alloy at 300 °C (40.5 %) is much higher than that of Gd-free alloy (10 %), which is very attractive for the application of Mg alloy at higher temperature. However, there is also a problem that the precipitates formed at a lower ageing temperature are very unstable at higher application temperatures, thus are not ideal for the high temperature applications. A traditional approach in solving the problem is from alloy design and development route by increasing solute concentrations or addition of micro-alloying elements. However, the low nucleation rate and rapid growth of precipitates during conventional ageing make it still difficult to control the precipitate microstructure in order to obtain a higher strength. High pressure torsion (HPT) is well known to be effective in modifying materials microstructures and achieving significant refinement in grain size [10]. Recently, HPT was also employed to tailor the precipitate microstructures of the age-hardening alloy that are significantly different from those obtained by conventional isothermal ageing treatments [11].

In this investigation, an Mg-6Zn-2Gd-0.4Zr (wt. %) alloy have been subjected to high pressure torsion. The precipitate microstructure evolution during HPT processing has been characterised carefully by using TEM, with an aim to elucidate the effect of HPT processing on nucleation and growth of precipitates, and the mechanisms dominating the evolution of precipitate microstructure.

Experimental material and procedures

The Mg-6Zn-2Gd-0.4Zr alloy (wt. %, used throughout the paper, in case not specified otherwise) was prepared from pure Mg (99.9%), Zn (99.9%), Mg–28Gd and Mg–33Zr master alloys in an electric resistance furnace under an anti-oxidizing flux as protection, and then cast into a sand mould at about 720 °C. Solution treatment was performed in a salt bath at 500 °C for 18 h, followed by quenching into cold water and then ageing in oil at 200 °C for 15 h.

Extrusion was perofrmed at room temperature with a pressing speed of 0.2 m/min, with an aim to break the large second phase, weak the texture, and make it possible to perform HPT at room temperature. After extrusion, final rod is about 15x15 mm² in size, and then the samples were machined with the diameters d = 8 mm, thickness t = ~ 0.8 mm. HPT was perofrmed at room temperature. Disks with the thickness around 0.8 mm and the diameter of 8 mm were processed for 1, 4, and 8 revolutions, under 1, 2, and 4 GPa, respectively, and a very low strain rate of about 10^{-2}/s. Hardness testing was performed with 50 N load and 15 sec dwell time. Each data point reported in this paper represents an average of at least 10 measurements.

Disks of 3 mm diameter were punched from thin strips cut from the HPT samples and they were ground carefully to a thickness of ~ 100 μm and dimpled to about 30 μm, and then ion-beam milled using a Gatan Precision Ion Polishing System (PIPS, Gatan model 691). Transmission electron microscopy (TEM) characterizations were performed using CM12 operating at 120 kV.

Results and discussions

Microstructure and precipitates before extrusion and HPT

Figure 1 shows microstructures of ZG62 alloy both in the as-cast condition and after a solution treatment. The microstructure of the as-cast sample was composed of equiaxed α-Mg grains surrounded by eutectic at triple junctions and grain boundaries, as shown in Figures. 1a, c. The mean grain size of the ZG62 alloy was measured to be approximately 35 μm using a linear intercept method. This grain size is similar to that observed in a ZK60 alloy with 1.3% Gd addition, but significantly less than that of ZK60 alloy (71 μm) [9]. This result is also consistent with other observations that the addition of Gd (less than 2 wt. %) refines the microstructure [8, 9]. After solution treatment at 500 °C for 18 h, the eutectic structures in ZG62 alloy almost dissolve but some discontinuous second phase particles survive on the grain boundary, as shown in Figures 1b, d. Energy dispersive X-ray (EDX) spectra of particles, as marked with white arrows shown in Figure 1 d, indicated the particles were enriched with Zn (about 17 wt. %, 9 at. %) and Gd (about 20 wt. %, 4 at. %), as shown in Figure 1e.

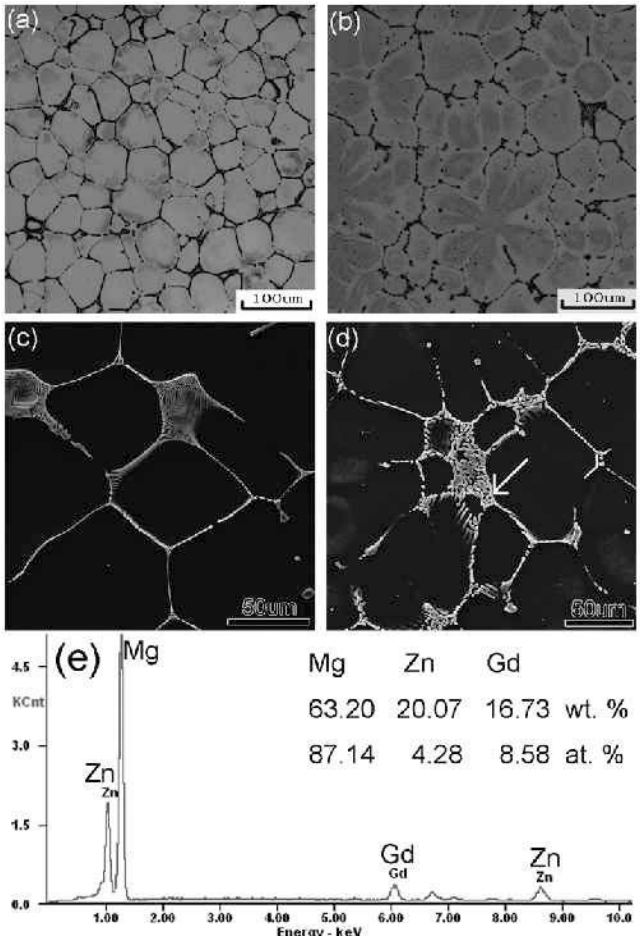

Figure 1 Microstructure of Mg-6Zn-2Gd-0.6Zr (wt. %) alloy. (a), (b), optical microscopy image; (c), (d), SEM image. (a), (c) as-cast; (b), (d) after a solution treatment at 500 °C for 18 h; (e) the energy dispersive X-ray (EDX) spectra analysis results of the particles, as marked in Figure 1 d.

After a solution treatment at 500 °C for 18 h and subsequent ageing at 200 °C for 15 h, some finer precipitates also observed in the α-Mg matrix. Figure 2 shows the $[01\text{-}11]_\alpha$, $[1\text{-}21\text{-}3]_\alpha$, $[01\text{-}10]_\alpha$ bright field TEM images (a), (c), (e) and corresponding SADPs (b), (d), (f) of the precipitates obtained from the ZG62 alloy aged at 200 °C for 15 h. Viewed from three different direction, it is clear that the precipitates with three different morphologies, i.e. $[0001]_\alpha$ rods/lath, $(0001)_\alpha$ plates and blocky particles, as marked with white arrows and labeled as 1, 2 and 3 in Figure 2e, are present in the α-Mg matrix. This is consistent with the observation in an Mg-Zn alloy [12, 13]. The $[0001]_\alpha$ rods (labeled as 1) have been commonly regarded as β_1', while the $(0001)_\alpha$ plates (labeled as 2) were commonly taken as β_2' in previous studies [3, 12-15]. Both β_1' and β_2' have a hexagonal structure (a=0.523nm, c=0.858nm) [12, 15], which is identical to that of Laves phase $MgZn_2$ [15].

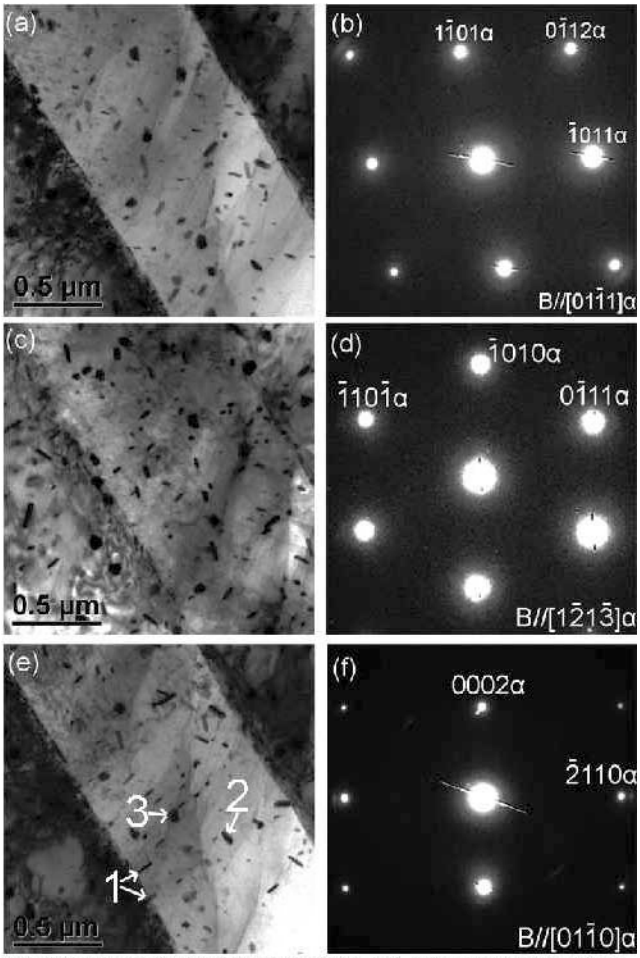

Figure 2 Bright field TEM images (a), (c), (e) and corresponding $[01\text{-}11]_\alpha$, $[1\text{-}21\text{-}3]_\alpha$, $[01\text{-}10]_\alpha$ SADPs (b), (d), (f) of the precipitates obtained from Mg-6Zn-2Gd-0.6Zr (wt. %) alloy aged at 200 °C for 15 h.

Microstructure and precipitates after extrusion and HPT

Figure 3 shows SEM images of the 1-GPa, 1, 4, and 8-revolution HPT sample (a, c, e taken from the centre (d < 2 mm), b, d and e taken from the edge (2 < d < 4 mm)). Fragmentation of the larger second phase was achieved after 1-revolution HPT, both in the centre and the edge, as shown in Fig. 3, compared to Figure 1 (as-cast and T4 heat treatment). Fragmentation of the larger second phase was believed to play a major role in precipitate evolution and this process is responsible for the spheroidization of precipitates during HPT [16,17].

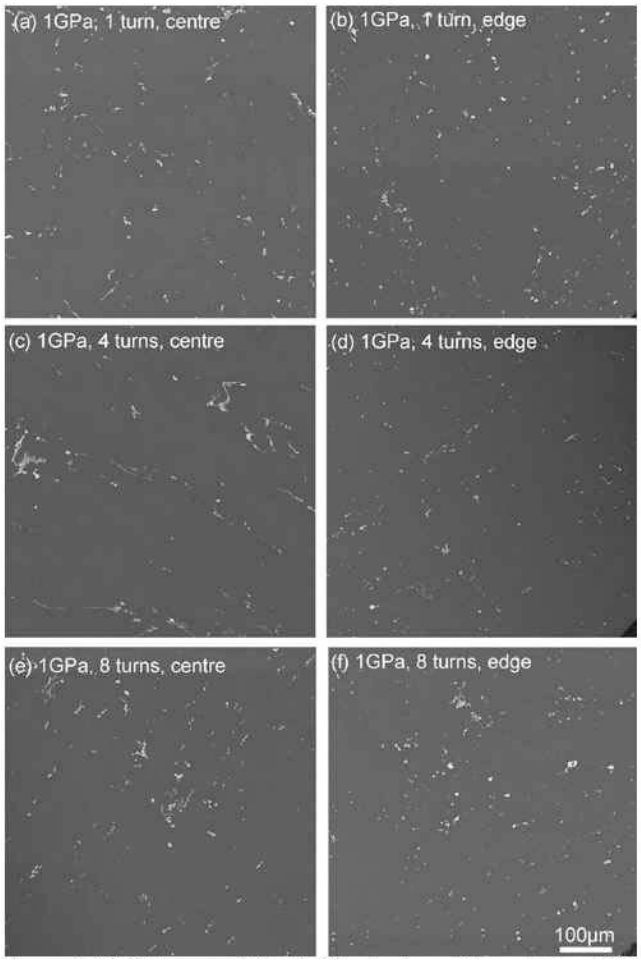

Figure 3 SEM images of the 1-GPa, 1, 4, and 8-revolution HPT sample (a, c, e were taken from the centre, b, d and e were taken from the edge).

Figure 4 shows SEM images of the 2, and 4-GPa, 8-revolution HPT sample (a, c were taken from the centre, b and d were taken from the edge). More significant fragmentation of the larger second phase was observed. Especially, at the edge, much finer and round particles were observed. These particles are about 500 nm in size (diameter), and are rich in Zn and Gd, as shown in Figure 5c. Furthermore, fragmentation of the small precipitates also occurs during HPT, as marked with a white arrow in Figuree 5a. The platelets precipitates were fragmented into small round particle (< 25 nm). As a result, the growth of the small precipitates will be restrained and no small platelets will have the capability to grow into larger precipitates. This is in contradiction with the many larger platelets, more than ~ 25 nm long, observed in T6 condition, as shown in Figure 2.

Examination of the sample after the 1-GPa, 8-revolution reveals a significant difference from that after the 1-GPa, 1-revolution. Figure 6 shows some TEM image (a, c) and corresponding SADP (b, d) of the 1-GPa, 8-revolution HPT sample taken from the centre (a, b) and the edge (c, d), respectively. In both cases (centre and edge), the microstrucutre seems to be much more homogeneous, although some small precipitates were still observed in the centre (Figure 6a), indicating that HPT (1-GPa, 8-revolution) can produce enough stains to tailor the precpitates. Most weak diffraction spots of the precipitates scatter randomly with many spots situated, as shown in Figures 6b and d, on the white ring. This indicates that these precipitates are distributed with random orientations in the matrix.

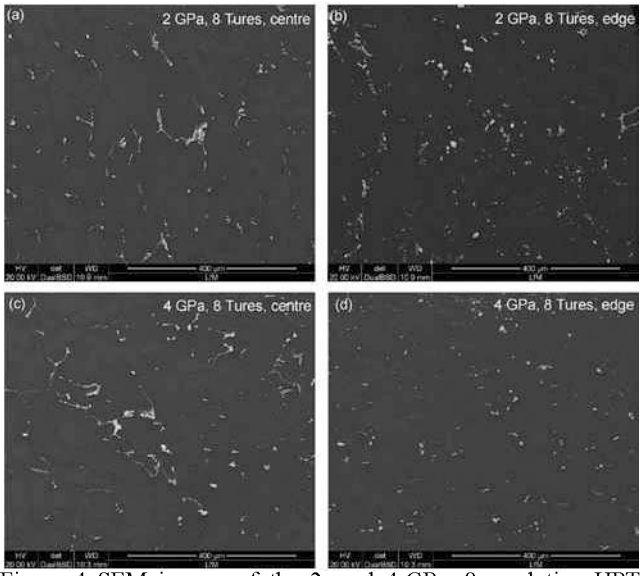

Figure 4 SEM images of the 2, and 4-GPa, 8-revolution HPT sample taken from the centre (a, c) and the edge (b and d).

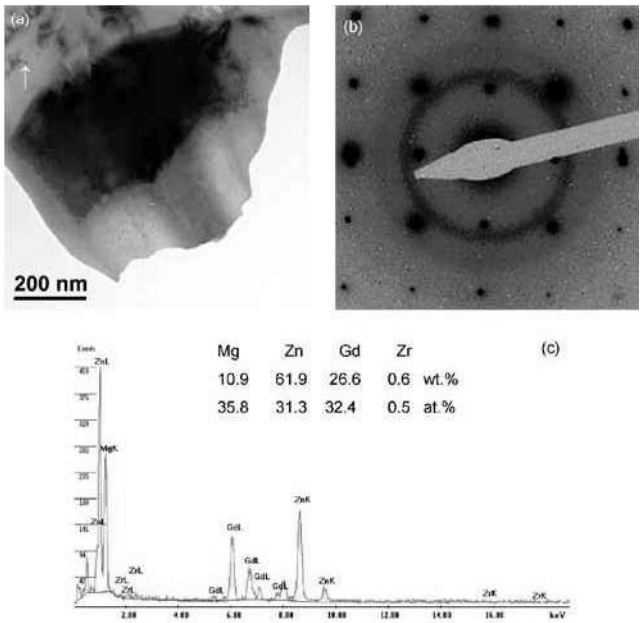

Figure 5 TEM image (a) and corresponding SADP (b), EDX analysis (c) of the 1-GPa, 1-revolution HPT sample taken from the centre.

Examination of the sample after the 4-GPa, 8-revolution , as shown in Figure 7, also reveals a significant difference from that after the 1-GPa, 8-revolution (Figures 6a, b). The higher pressure (4-GPa compared to 1-GPa) may result into a increasing temperature during HPT, which can promote the "second" precipitation during HPT. It seems that the precipitates are probably undergoing coalescence. Indeed, if the growth of large precipitate is predominantly via coalescence rather than by the dissolution of smaller precipitates, no small precipitates are

expected to exist at the areas remote from these larger precipitates, as shown in Figure 7c, where a "precipitation free zone" was observed along the large plate-like precipitates.

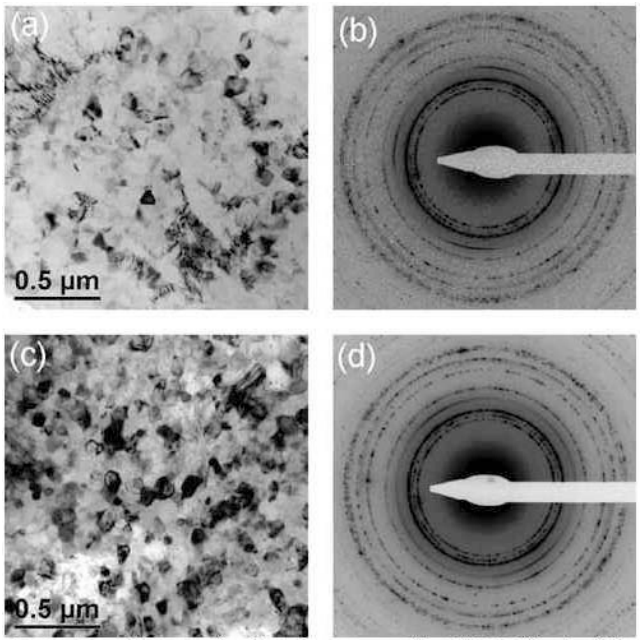

Figure 6 TEM image (a, c) and corresponding SADP (b, d) of the 1-GPa, 8-revolution HPT sample taken from the centre (a, b) and the edge (c, d).

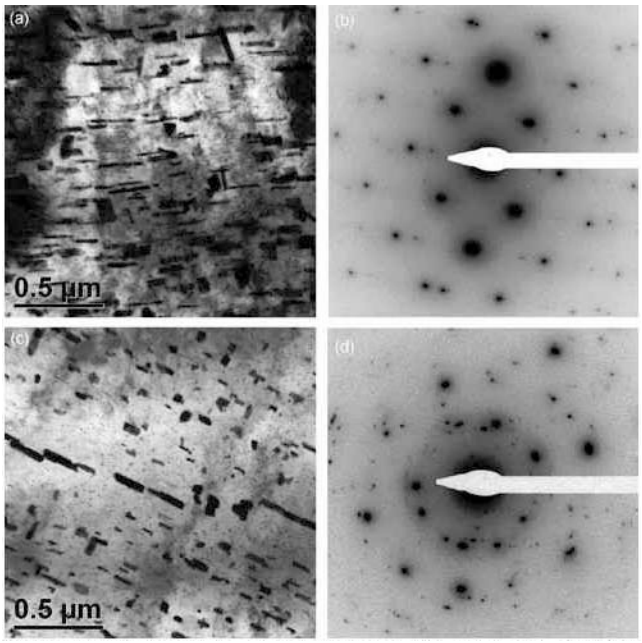

Figure 7 TEM image (a, c) and corresponding SADP (b, d) of the 4-GPa, 8-revolution HPT sample taken from the centre.

As expected, examination of microstructure taken from the edge of the HPTed sample after the 4-GPa, 8-revolution also reveals a significant difference from that taken from the centre. Figure 8 shows TEM image (a, c) and corresponding SADP (b, d) of the 4-GPa, 8-revolution HPT sample taken from the edge. In contrast to

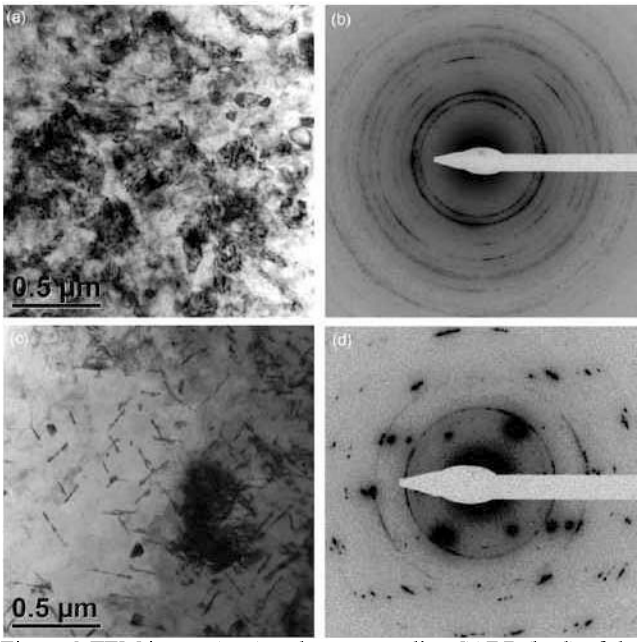

Figure 8 TEM image (a, c) and corresponding SADP (b, d) of the 4-GPa, 8-revolution HPT sample taken from the edge.

the centre (Figure 7), most weak diffraction spots of the precipitates scatter randomly with many spots situated, as shown in Figure 8b and d, on the white ring. This is fully consistent with the observation in the HPTed sample after the 1-GPa, 8-revolution (Figure 6). Also, this indicates again that these precipitates are distributed with random orientations in the matrix after 8-revolution. Thus, it is very clear that the accumulated strain imposed by HPT significantly alters the orientations of the precipitates away from their initial preferred orientations. Furthermore, it is also very clear that HPT causes significant fragmentation of the large precipitates and increases their appearance within the matrix, as shown in Figure 8c. Sub-grains with small angle sub-grain boundaries are rare in the centre of 4-GPa, 8-revolution HPT sample, and are no longer seen in the edge of 4-GPa, 8-revolution HPT sample, suggesting that, with the further deformation, grain orientation continued until all the sub-grains had the same orientation and the sub-grain structure disappeared to form a larger grain. This difference between the centre and edge is also consistent with the fact that the deformation is not homogeneous in the through-thickness direction during HPT. The heterogeneous nature of flow during HPT is probably due to local variations in the flow stress of the sample during HPT processing [18].

In the case of the 1-GPa, 1-revolution sample, dislocations are seen with high density at sub-grain boundaries to accommodate the small angle misorientations between neighboring sub-grains but are hardly seen within each sub-grain, indicating that grain rotation plays a primary role in the early stage of the HPT process. At the initial stage of the HPT process grain rotation first converted high-angle grain boundaries to low-angle grain boundaries, forming large grains with sub-grains consisting of initial small grains. In contrast, in the case of 1-GPa, 8-revolution HPT sample (Figure 6) and 4-GPa, 8-revolution HPT sample (Figure 8), high density of dislocations is observed in the grains and this can be easily seen through the strong contrast variation caused by the strain field around dislocations in grains which are in a strong diffraction condition (i.e., the grains appear dark), as

shown in Figure 6c and Figure 8a. The high density of dislocations found in the 1-GPa, 8-revolution HPT sample and 4-GPa, 8-revolution HPT sample indicates that dislocations play a primary role in accommodating the deformation process at this stage. In other words, during HPT at higher revolutions dislocation slip became the primary deformation mechanism, in which dislocation accumulation and dynamic recovery reached a dynamic balance [19].

Hardness after T6, extrusion and HPT

Figure 9 shows hardness values measured at different processting conditions and positions. As expected, the hardness increases slightly after extrusion. The increasing hardness can be attributed to the grain refinement caused by the extrusion. However, unexpectedly, the hardness does not increase greatly after HPT, as compared to the extrusion condition. Furthermore, in some cases (1-GPa, 1-revolution; 4-GPa, 1-revolution), the hardness is less than that in the extrusion condition. This indicates that increasing strain may lead to a continuous grain growth, and thus a lower hardness due to the Hall-Petch effect [20].The higher, but relatively stable hardness was achieved after 1-GPa, 4-, 8-revolution, and 4-GPa, 4-, 8-revolution. This indicates that increasing revolution may result in an equilibrium structure, supporting a dynamic balance between deformation-induced grain growth and grain refinement and between deformation-induced dislocation generation and dislocation annihilation [21]. This is also fullyconsistent with the microstructure observation (Figures 6-8). The higher hardness can be attributed to the promotion of heterogeneous nucleation of the precipitates, and suppress of its growth amazingly caused by the high strains during HPT, similar to the case of ECAPed Mg-Nd-Gd based alloy [22]. It can be also expected that ductility will be improved greatly without sacrificing of strength. Further investigation on mechanical properties is in progress.

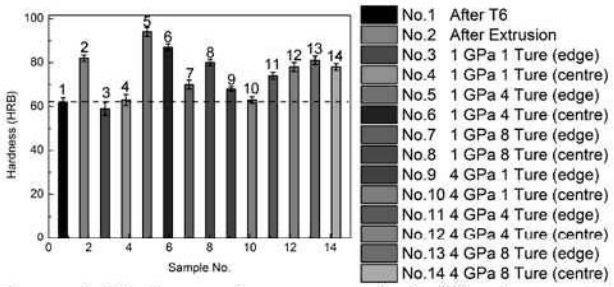

Figure 9 Hardness values measured at different processting condition and position.

Conclusions

HPT has been employed to tailor the precipitate microstructures in ZG62 alloy. An enhanced aged hardening response was achieved due to the promotion of heterogeneous nucleation of the precipitates, and suppress of its growth amazingly caused by the high strains during HPT. This research demonstrates a new perspective for application of HPT to tailor precipitate microstructure for unique properties in service.

Acknowledgements

Jiehua Li gratefully acknowledges Prof Gerhard Dehm for his access to TEM and Prof Pippan Reinhard for his help on HPT at the Erich Schmid Institute of Materials Science of the Austrian Academy of Science.

References

[1] B. Smola, I. Stulíková, F. von Buch, and B.L. Mordike, "Structural aspects of high performance Mg alloys design," *Mater. Sci. Eng. A*, 324 (2002), 113-117.

[2] J.B. Clark, "Transmission electron microscopy study of age hardening in a Mg-5 wt.% Zn alloy," *Acta Metall.*, 13 (1965), 1281-1289.

[3] J.B. Clark, L. Zabdyr, and Z. Moser. "Binary Alloy Phase Diagram," 2nd ed. T.B. Massalski, H. Okamoto, P.R. Subramanian and L. Kacprzak (ASM International, Metals Park, OH, 1988), 2571-2572.

[4] J.F. Nie, X. Gao, and S.M. Zhu, "Enhanced age hardening response and creep resistance of Mg–Gd alloys containing Zn," *Scripta Mater.*, 53 (2005), 1049-1053.

[5] X. Gao, and J.F. Nie, "Enhanced precipitation-hardening in Mg–Gd alloys containing Ag and Zn," *Scripta Mater.*, 58 (2008), 619-622.

[6] J.F. Nie, K. Oh-ishi, X. Gao, and K. Hono, "Solute segregation and precipitation in a creep-resistant Mg–Gd–Zn alloy," *Acta Mater.*, 56 (2008), 6061-6076.

[7] J.H. Li, and P. Schumacher, "Solidification and age hardening behaviour of Mg-Zn-Gd Alloys," *IOP Conf. Series: Materials Science and Engineering*, 27 (2011), 012021.

[8] J. Yang, L.D. Wang, L.M Wang, and H.J. Zhang, "Microstructures and mechanical properties of the Mg–4.5Zn–*x*Gd (*x* = 0, 2, 3 and 5) alloys," *J. Alloys Compd.*, 459 (2008), 274-280.

[9] S.M. He, L.M. Peng, X.Q. Zeng, W.J. Ding, and Y.P. Zhu, "Comparison of the microstructure and mechanical properties of a ZK60 alloy with and without 1.3 wt.% gadolinium addition," *Mater. Sci. Eng. A*, 433 (2006) 175-181.

[10] A. P. Zhilyaev, G.V. Nurislamova, B. K. Kim, M.D. Baró, J.A. Szpunar, and T. G. Langdon, "Experimental parameters influencing grain refinement and microstructural evolution during high-pressure torsion," *Acta Mater.*, 51 (2003), 753-765.

[11] G. Sha, Y.B. Wang, X.Z. Liao, Z.C. Duan, S.P. Ringer, and T.G. Langdon, "Influence of equal-channel angular pressing on precipitation in an Al–Zn–Mg–Cu alloy," *Acta Mater.*, 57 (2009), 3123-3132.

[12] L.Y. Wei, G.L. Dunlop, and H. Westengen, "Precipitation Hardening of Mg-Zn and Mg-Zn-RE alloys," *Metall. Mater. Trans. A*, 26 (1995), 1705-1716.

[13] X. Gao, and J.F. Nie, "Characterization of strengthening precipitate phases in a Mg–Zn alloy," *Scripta Mater.*, 56 (2007), 645-648.

[14] L.L. Rokhlin, and A.A. Oreshkina, *Fiz. Metal. Metalloved.* 66 (1988), 559.

[15] Y. Komura, and K. Tokunaga, "Structural studies of stacking variants in Mg-base Friauf-Laves phases," *Acta Crystallogr.*, 36B (1980), 1548-1554.

[16] J. Gubicza, I. Schiller, N.Q. Chinh, J. Illy, Z. Horita, and T.G. Langdon, "The effect of severe plastic deformation on precipitation in supersaturated Al–Zn–Mg alloys," *Mater Sci Eng A*, 460-461 (2007), 77-85.

[17] K. Matsubara, Y. Miyahara, Z. Horita, and T.G. Langdon, "Developing superplasticity in a magnesium alloy through a

combination of extrusion and ECAP," *Acta Mater.*, 53 (2005), 749.

[18] R. B. Figueiredo, P. R. Cetlin, and T. G. Langdon, "Using finite element modeling to examine the flow processes in quasi-constrained high-pressure torsion," *Mater Sci Eng A*, 528 (2011), 8198-8204.

[19] Y.B. Wang, J.C. Ho, X.Z. Liao, H.Q. Li, S.P. Ringer, and Y.T. Zhu, "Mechanism of grain growth during severe plastic deformation of a nanocrystalline Ni–Fe alloy," *Appl. Phys. Lett.*, 94 (2009), 011908.

[20] R.Z. Valiev, "Nanomaterial Advantage," *Nature*, 419 (2002), 887-889.

[21] S. Ni, Y.B. Wang, X.Z. Liao, S.N. Alhajeri, H.Q. Li, Y.H. Zhao, E.J. Lavernia, S.P. Ringer, T. G. Langdon, and Y.T. Zhu, "Grain growth and dislocation density evolution in a nanocrystalline Ni–Fe alloy induced by high-pressure torsion," *Scripta Mater.*, 64 (2011), 327-330.

[22] G. Sha, J.H. Li, W. Xu, K. Xia, W.Q. Jie, and S.P. Ringer, "Hardening and microstructural reactions in high-temperature equal-channel angular pressed Mg–Nd–Gd–Zn–Zr alloy," *Mater Sci Eng A*, 527 (2010), 5092-5099.